Design, takeoff and steering torques modulation of an 80-mg insect-scale flapping-wing robot

Chenyang Wang, Weiping Zhang ✉, Jiaxin Zhao, Junqi Hu, Yang Zou

National Key Laboratory of Science and Technology on Micro/Nano Fabrication, School of Electronic Information and Electrical Engineering, Shanghai Jiao Tong University, Shanghai 200240, People's Republic of China
✉ *E-mail: zhangwp@sjtu.edu.cn*

Published in Micro & Nano Letters; Received on 24th June 2020; Revised on 22nd September 2020; Accepted on 3rd November 2020

An 80-mg double piezo-actuated insect-inspired flapping-wing robot is presented in this Letter. With the design of the two piezoelectric actuators placed back to back, each wing of this robot is independently driven and controlled, giving this robot the ability to achieve asymmetric flapping of the two wings to generate torques for steering. The piezoelectric actuators are designed with electrical insulation and structural reinforcement to improve the reliability under high-voltage and high-frequency drive mode. Fibre directions of each component of the robot are reasonably designed to enhance strength and stiffness. The average lift generated by the robot is measured by a customised lift measurement system found to be proportional to the square of the input voltage amplitude. The three steering torques generated by the robot are measured separately by a customised lift measurement system. Each steering torque can only be linearly modulated by its specific control variable of the input voltages. With a total weight of 80 mg and a wingspan of 3.5 cm, this robot can generate sufficient lift to take off and independently modulate all three steering torques with good decoupling, which is vital for the further controlled flight.

1. Introduction: Up to now, several insect-scale (generally wingspan < 5 cm, weight < 5 g) flapping-wing robots have successfully achieved takeoff against their gravity [1–6]. Furthermore, researchers have begun to focus on the multi-degree flight control of the insect-scale flapping-wing robot. RoboBee, developed by Harvard University, has successfully achieved the first controlled flight of the insect-scale flapping-wing robot based on the external power supply and control system [7]. Bee^{+}, a 95-mg four-winged microrobot developed by the University of Southern California uses the torques modulation similar to the quadrotors to achieve hovering [8].

In [5], we demonstrated a piezo-actuated insect-inspired flapping-wing robot which weighs 84 mg with a wingspan of 35 mm and can generate sufficient thrust to take off. However, the design of single actuator causes the two wings of this robot to flap only symmetrically, which results in a condition where only the pitch torque can be adjusted and the full-degree-of-freedom steering of the robot cannot be adjusted. Following the design method and the microfabrication we presented in [5, 6], a redesigned insect-scale flapping-wing robot is presented in this Letter to focus on the steering issue. This insect-scale flapping-wing robot utilises two piezoelectric actuators as the power sources to control the two wings independently, that is, the asymmetric flapping of the two wings can be achieved. As a result, this robot can takeoff against gravity and generate all three (roll, pitch, and yaw) torques for steering with good decoupling.

2. Overall design and fabrication: The insect-scale flapping-wing robot consists of two piezoelectric actuators, a transmission consisting of two sets of spherical four-bars, a pair of wings and airframe, as shown in Fig. 1. All of these separate components are shaped by ultraviolet (UV) laser in two-dimension and then assembled in a certain order with the help of the airframe. This robot uses two piezoelectric actuators as input to drive wings to flap through a set of transmission, as shown in Fig. 1*a*. Specifically, excited by specific AC driving voltage, the actuator tip (made of glass fibre) produces reciprocating movement caused by the deformation of the two-layer $PbZrTiO_3$, as shown in Fig. 2*a*. Since the reciprocating amplitude of the actuator tip is too small to directly drive the wing, and the desired stroke plane of the flapping wing is perpendicular to the stroke plane of the reciprocating tip, the spherical four-bar transmission based on the flexible hinge is introduced to transform the input reciprocating movement of the actuator tip into the output flapping of the wing, as shown in Fig. 2*b*. By the non-rigid connection of flexible hinge on the wing root, the wing will produce passive rotations under an aerodynamic moment, which are the main factors for the generation of lift force. It is worth noting that the two wings of this robot are independently driven by two piezoelectric actuators as shown in Fig. 3, so that the pitch, roll and yaw torques can be generated and modulated by the asymmetric flapping of the two wings, which is necessary for controlled fight.

The piezoelectric actuator used in this robot is modified from the actuator used in [5] as shown in Fig. 4*a*. First, the piezoelectric actuator used in this robot is narrower than the one used in [5] since a single actuator is only used to drive one wing in this robot, and the head of the actuator (especially the tip of the head) is further narrowed to reduce the dynamic load of the actuator while vibrating at high frequency and concentrate the output force on the tip to improve the driving efficiency. Second, the plug of the actuator head used for assembly with the plane four-bar transmission, originally located on the actuator's tip, is replaced to the side of the actuator head to match the spherical four-bar transmission. Since the tail of the actuator needs to be firmly fixed on the airframe, the tail is designed with two holes and a plug for assembly with the airframe to avoid the vibration caused by loose fixation. In addition, the actuator needs to drive the wing to flap at high frequency under high voltage. To improve the reliability of the actuator, glass fibre is used in both ends of the actuator to electrically isolate itself from the other components, and strengthen the rigidity of the actuator's tail and head.

The similar structural design and microfabrication process of the piezoelectric actuator in [5] is used in this robot. As shown in Fig. 4*b*, each piezoelectric actuator consists of seven flat sheets, including two sheets of 127 μm thick $PbZrTiO_3$, a sheet of 40 μm thick carbon fibre, and four sheets of 120 μm thick glass fibre. The sheet of carbon fibre is used to bond the two sheets of $PbZrTiO_3$ and act as the conductive layer. The four sheets of

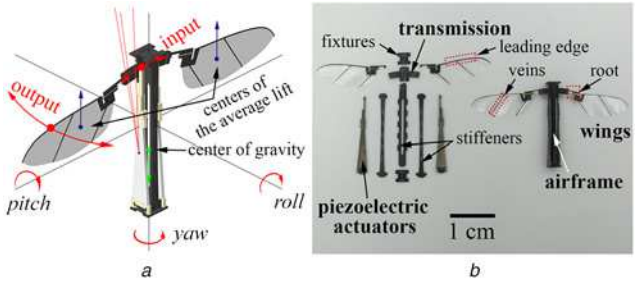

Fig. 1 *The 80-mg insect-scale flapping-wing robot*
a CAD model of the robot
b Robot and all its components

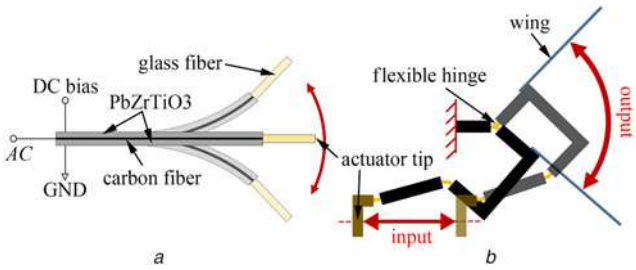

Fig. 2 *Each wing is driven independently by a piezoelectric actuator through the spherical four-bar transmission*
a Working principle of the piezoelectric actuator
b Working principle of the spherical four-bar transmission (top view)

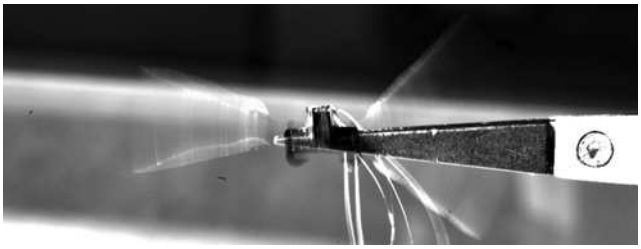

Fig. 3 *Asymmetrical flapping of the two wings of the designed robot*

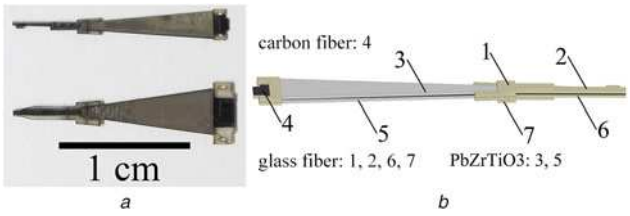

Fig. 4 *The modified piezoelectric actuator*
a Piezoelectric actuators used in this robot (up) and in [5] (down)
b Seven flat sheets of the piezoelectric actuator

glass fibre are used to act as the rigid extension, electrical insulation and structural support. The fibre direction of each sheet of glass fibre and carbon fibre is deliberately designed to be along the vibration direction of the actuator for higher strength. Finally, the piezoelectric actuator is shaped and released by a UV laser. Excited by the electric field, the two sheets of $PbZrTiO_3$ are deformed mechanically and thus the driving force is generated. The two piezoelectric actuators are placed back to back to offset the torque in the case of opposite vibration. It is noteworthy that the structure of the two piezoelectric actuators is mirror symmetrical as shown in Fig. 1*b*.

Fig. 5 *Photograph of the transmission before and after folding*

Considering that the two piezoelectric actuators used in this robot are placed back to back if the transmission follows the design of the planar four-bar mechanism used in [5], the 'thorax' structure of this robot will become bloated. Inspired by [7, 9], a spherical four-bar mechanism is used as the transmission to convert the displacement of the tip of the actuator into the flapping of the wing. To be noticed that the two piezoelectric actuator serves as two rotary sources. According to the kinematics of the spherical four-bar mechanism, all joints of the transmission meet at the centre of the virtual rotary axis of the piezoelectric actuator, as the red lines shown in Fig. 1*a*. The same microfabrication of the flexible hinge introduced in [5, 10] is used for the spherical four-bar transmission in this robot. The transmission is shaped and released by UV laser in two-dimension, and then folded and glued into three-dimension, as shown in Fig. 5. To be noticed, the shape of the transmission is deliberately designed with long arc length and narrow width. By the design of the long arc length, the space between the flexible hinges is slightly increased to avoid the thermal effects of laser processing for a more accurate and stable transmission ratio. Besides, the dynamic load of the transmission is reduced with the narrow width.

The artificial wing used in this robot is the same as the wing used in [5], which is designed to imitate the wings of drone-fly *Eristalis tenax* [11] in similar size and shape. The leading edge, veins and root of the wing designed to be as slim as possible for lightweight, as shown in Fig. 1*b*. To ensure sufficient strength, these components of the wing are patterned in different 60-μm thick carbon fibre sheets, and the fibre direction of each sheet is deliberately arranged. The 1.5-μm thick polyester is used as the wing membrane. As the result, a single wing weighs 0.5 mg and is 13-mm long.

The airframe is used to support two separate drive mechanisms and realise the decoupling of wing kinematics, which is required to be solid and light enough. In this robot, the airframe is composed of three vertical stiffeners and two horizontal fixtures made of two sheets of 80-μm thick carbon fibre shown in Fig. 1*b*, among which the fibre directions of the stiffeners are parallel and the fibre directions of the fixtures are orthogonal for higher stiffness.

In addition, the assembly position of the wings and the transmission is deliberately designed to make the centre of gravity of the robot located on the geometric centre axis of the prototype, and in the same plane as the centre of the average lift generated by each wing as shown in Fig. 1*a*. The centre of gravity of the robot is slightly lower than the centre of the average lift. Therefore, the passive stability of the robot is improved by these designs.

Table 1 Mass of the components

Component	Mass, mg
double actuators	56
transmission and airframe	15
double wings	1
wiring, epoxy	8
total	80

doi: 10.1049/mnl.2020.0371

As a result, the corresponding weight of each component of the entire robot is shown in Table 1.

3. Experiments

3.1. Lift measurement for the robot: The lift produced by the robot is only in mN-scale, which cannot be directly measured by current commercial force sensors, a customised lift measurement system is designed for the robot referring to [12]. As shown in Fig. 6*a*. The lift of robot is transformed into a slight parallel displacement along measurement direction of a capacitive displacement sensor (CS005, MICRO-EPSILON) by the Invar-made double-cantilever beam, thus the real-time lift can be derived by measuring the displacement of the target plate. After calibration, the lift measurement system has a stiffness of 457 N/m, a dynamic resolution of 0.46 μN, and a sensitivity of 2.19 μm/mN.

As shown in Fig. 6*b*, the robot is mounted to the lift measurement system through a long truss made of carbon fibre to avoid the influence of airflow while flapping. Based on the test methods of the piezoelectric actuator introduced in [5], the resonant frequency of the robot is measured as 100 Hz. Thus, a sinusoidal voltage with a fixed frequency of 100 Hz is applied to the two actuators for the highest energy efficiency [13]. By modulating the input voltage amplitude V_{amp}, the corresponding change in the average lift is shown in Fig. 7, showing that the average lift generated by the robot is proportional to the square of V_{amp}, and the average lift exceeds the gravity of the robot when V_{amp} is >94 V. However, the lift tends to reach saturation when V_{amp} is >90 V, because the spherical four-bar is close to its limit position at this time, limiting the further increase of the flapping angle of the two wings. As shown in Fig. 8, applied by a sinusoidal voltage with a frequency of 100 Hz and amplitude of 120 V, the robot takes off against gravity along the rails vertically.

3.2. Steering torques modulation of the robot: The magnitude of the steering torque generated by this robot is generally around μNm,

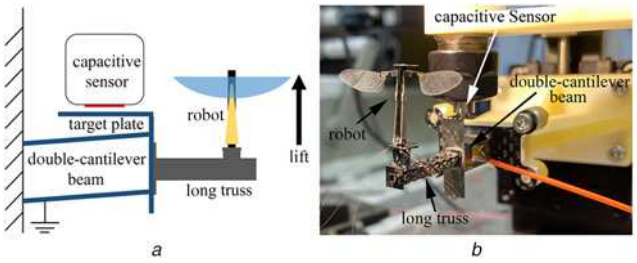

Fig. 6 *The customised lift measurement system for the robot*
a Schematic representation of the customised lift measurement system
b Robot mounted on the lift measurement system through a long truss

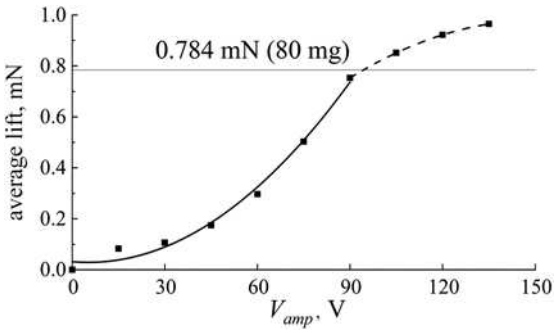

Fig. 7 *Measured relationship between the average lift and the input voltage amplitude of the robot. The solid and dashed lines are the quadratic fit from 0 to 90 V and 90 to 135 V, respectively. Each point is averaged over 100 cycles of filtered real-time lift*

Fig. 8 *Liftoff of the robot. The interval between the images is approximately 1 s*

which cannot be measured directly by current commercial torque sensors. Thus, a customised torque measurement system used for the robot is built referring to [14]. As shown in Fig. 9, the torque acting along the axis of the cross-shaped Invar-made beam causes the beam to rotate slightly, which can be regarded as a parallel displacement for a small rotation. The same capacitive displacement sensor for the lift measurement is used to measure the displacement of the target plate on the cross-shaped beam; the real-time torque can be then derived. After calibration, the torque measurement system has an actual torsional stiffness of 94.4 mNm/rad, a dynamic resolution of 0.01 μNm, and a sensitivity of 90.27 mm/Nm. The experimental setup of the customised torque measurement system is shown in Fig. 10*a*, a long truss is also used to avoid the influence of airflow while flapping. In this case, the pitch torque is measured. For the roll and yaw torques measurement, the robot needs to be remounted to make its rotation axis parallel to the sensing direction of the system, as shown in Figs. 10*b* and *c*.

3.2.1. Roll: The roll torque of the robot is caused by the lift difference generated by the left and right wings, as shown in Fig. 11*a*. The amplitudes of the voltages applied to the left and

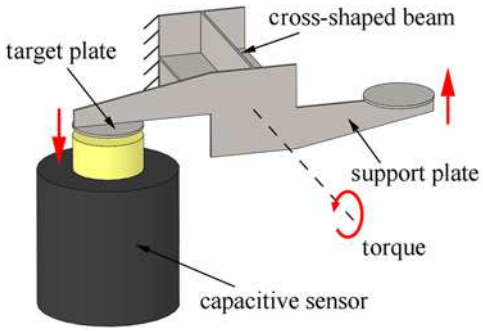

Fig. 9 *Schematic representation of the customised torque measurement system*

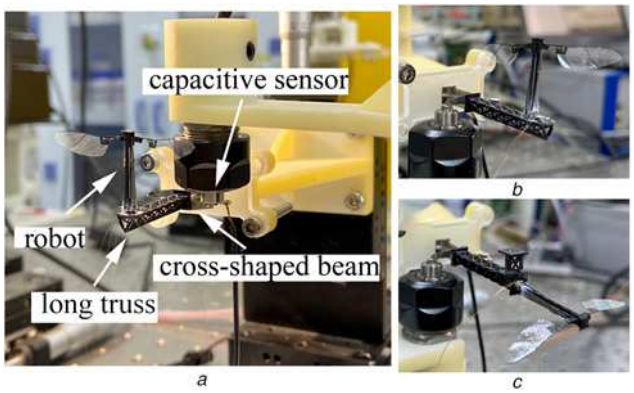

Fig. 10 *Different setup of the customised torque measurement system for specific steering torque*
a Setup of the roll torque measurement
b Mounting of the robot for pitch torque measurement
c Mounting of the robot for the yaw torque measurement

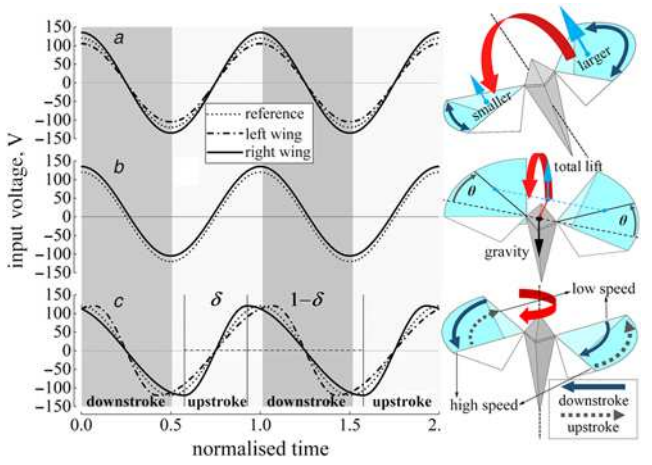

Fig. 11 *Mechanism of torques modulation*
a Roll: The difference in input voltage amplitude of the left and right wings causes the mean lift generated by the two wings to be different, then the roll torque is generated
b Pitch: The flapping plane of the two wings is shifted with an angle of θ when the input voltage of the two wings is raised, thus the pitch torque is generated by the offset between the centre of the total lift and gravity of the robot
c Yaw: The left-wing flaps faster than the right-wing during the downstroke and slower than the right-wing during the upstroke, resulting in a continuous difference in the drag force acting on the two wings, and then the yaw torque is caused

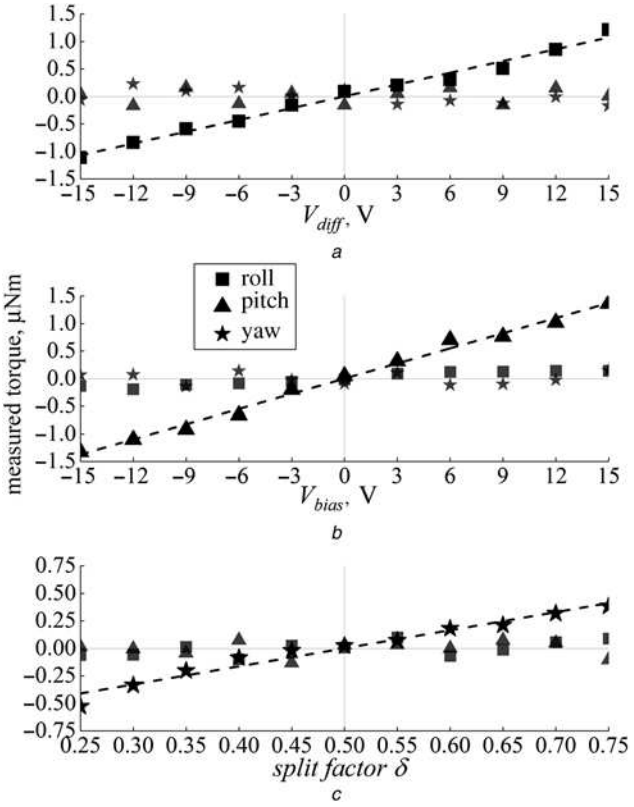

Fig. 12 *Each modulated torque is almost proportional to its control variable and insensitive to the control variables of the other two torques. The three dashed lines are the linear fit of the measured points of the three modulated torques*
a Roll
b Pitch
c Yaw

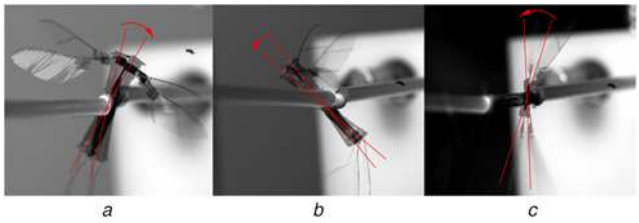

Fig. 13 *Movements of*
a Roll
b Pitch
c Yaw. The rotation of the robot is constrained to a specific degree of freedom for clarity

right actuators can be expressed by the basic amplitude $V_{amp,basic}$ and the amplitude difference V_{diff} as $V_{amp,left} = V_{amp,basic} + V_{amp,basic}$ and $V_{amp,right} = V_{amp,basic} - V_{amp,basic}$, respectively. By adjusting V_{diff}, the roll torque can be modulated. Applied by two sinusoidal signals with a fixed frequency of 100 Hz and $V_{amp,basic}$ of 120 V, the average roll torque is measured to be proportional to the amplitude difference between the two signals as shown in Fig. 12*a*. The roll movement of the robot is shown in Fig. 13*a*. In this case, the robot is applied with two sinusoidal signals with a fixed frequency of 100 Hz, $V_{amp,basic}$ of 120 V and V_{diff} of 10 V, resulting in the larger average lift generated by the left-wing, and then the robot rotates clockwise.

3.2.2. Pitch: The pitch torque of the robot is caused by the offset between the centre of the total lift and gravity of the robot, as shown in Fig. 11*b*. By adjusting the DC bias V_{bias} of the voltage applied to two actuators, the pitch torque can then be modulated. A sinusoidal control signal with a fixed frequency of 100 Hz and an amplitude of 120 V is applied to both of the actuators. By adjusting the DC bias V_{bias} of the sinusoidal control signal, the average pitch torque is measured to be proportional to the DC bias of the sinusoidal control signal as shown in Fig. 12*b*. The pitch movement of the robot is shown in Fig. 13*b*. In this case, the robot is applied by a sinusoidal signal with a fixed frequency of 100 Hz, $V_{amp,basic}$ of 120 V and V_{bias} of 10 V, causing the flapping plane of the two wings to shift to the right, and then the robot rotates counterclockwise.

3.2.3. Yaw: The yaw torque is caused by the difference in the drag force acting on the left and right wings: the drag force acting on the faster flapping wing is larger than the slower in a half flapping stroke. Inspired by the split-cycle constant-period frequency modulation (SCCPFM) [15], the frequency of the upstroke control signal of the right-wing is higher than that of the downstroke as shown in Fig. 11*c*, resulting in the upstroke flapping velocity of controlled right-wing faster than the downstroke, which is the opposite of the left-wing controlled by the complementary control signal. Thus, the continuous yaw torque in the same direction is generated since the faster half stroke and the slower half stroke of the two wings are periodically alternated. The split factor δ is introduced to describe how 'split' the control signal is. To be noticed, since the fundamental frequency of the complete control signal does not change, the resonance effect of the robot is not affected.

Two SCCPFM control signals with a fixed frequency of 100 Hz and amplitude of 120 V are applied to both of the actuators. As a result, the average pitch torque is measured to be proportional to the split factor δ of the control signals as shown in Fig. 12*c*. The yaw movement of the robot is shown in Fig. 13*c*. In this case, the robot is applied by two signals with a fixed frequency of 100 Hz, $V_{amp,basic}$ of 120 V and δ of 0.3, causing the robot to rotate counterclockwise due to the continuous difference in the drag force acting on the two wings.

doi: 10.1049/mnl.2020.0371

3.2.4. Analysis of coupling: The modulation of the three torques used for this robot is ideally decoupled from each other, which needs to be verified by experiments. Taking the roll torque as an example, since the torque measurement system has only one degree of freedom, the changes of the torques of pitch and yaw during exactly the same modulation of roll torque are measured separately to quantify the coupling of the specific control variable of the roll with the other two torques.

As shown in Fig. 12, when each torque is modulated independently, the changes of the other two torques are small. Therefore, this robot is capable of all three control torques modulation with good decoupling, which is helpful for further flight control.

4. Conclusions: Previous research focused on the design method and microfabrication of a sub-100 mg insect-inspired flapping-wing robot [5], this robot can take off against gravity but cannot generate sufficient steering torque to adjust the flight attitude since only one piezoelectric actuator was used. As a continuing study, a double piezo-actuated 80 mg insect-inspired flapping-wing robot is presented in this Letter to research on the modulation of steering torques. In this robot, each wing is independently driven by two redesigned piezoelectric actuators, giving the robot the ability to generate all three steering torques only by the asymmetric flap of the two wings. Each component of the robot is designed compactly to reduce weight as much as possible. Glass fibre is used for both electrical isolation and structural reinforcement of the two piezoelectric actuators to improve the reliability under high-voltage and high-frequency drive mode. In addition, the fibre directions of all these components are reasonably designed to enhance strength and stiffness. In addition, the average lift generated by the robot is measured by a customised lift measurement system and found to be proportional to the square of the input voltage amplitude. Excited by the control signal with the resonance frequency of 100 Hz and amplitude of 250 V, this robot is able to take off vertically against gravity. In particular, all three steering torques generated by the robot and the coupling between them are measured separately by a customised torque measurement system, and the movement of the robot under each torque is exhibited. It is shown that each steering torque can be independently modulated by its specific control variable and has good decoupling from the other two torques, which is expected to achieve controlled flight in the future.

5. Acknowledgments: This research was supported by the Supporting Foundation of the Ministry of Education of the People's Republic of China (grant nos. 6141A02022607, 6141A02022627), the Shanghai Science and Technology Commission Project (grant no. 19511104202), the Shanghai Professional technical service platform (grant no. 19DZ2291103), and the Pre-research Fund (grant no. 17070107).

6 References

[1] Wood R.J.: 'The first takeoff of a biologically inspired at-scale robotic insect', *IEEE Trans. Robot.*, 2008, **24**, (2), pp. 341–347
[2] Hines L., Campolo D., Sitti M.: 'Liftoff of a motor-driven, flapping-wing microaerial vehicle capable of resonance', *IEEE Trans. Robot.*, 2013, **30**, (1), pp. 220–232
[3] Roll J.A., Cheng B., Deng X.: 'An electromagnetic actuator for high-frequency flapping-wing microair vehicles', *IEEE Trans. Robot.*, 2015, **31**, (2), pp. 400–414
[4] Zou Y., Zhang W., Zhang Z.: 'Liftoff of an electromagnetically driven insect-inspired flapping-wing robot', *IEEE Trans. Robot.*, 2016, **32**, (5), pp. 1285–1289
[5] Zou Y., Zhang W., Ke X., *ET AL.*: 'The design and microfabrication of a sub 100 mg insect-scale flapping-wing robot', *Micro Nano Lett.*, 2017, **12**, (5), pp. 297–300
[6] Zou Y., Zhang W., Zhou S., *ET AL.*: 'Monolithic fabrication of an insect-scale self-lifting flapping-wing robot', *Micro Nano Lett.*, 2018, **13**, (2), pp. 267–269
[7] Ma K.Y., Chirarattananon P., Fuller S.B., *ET AL.*: 'Controlled flight of a biologically inspired, insect-scale robot', *Science*, 2013, **340**, (6132), pp. 603–607
[8] Yang X., Chen Y., Chang L., *ET AL.*: 'Bee^{+}: a 95-mg four-winged insect-scale flying robot driven by twinned unimorph actuators', arXiv preprint arXiv:1905.02253v2, 2019
[9] Hines L.L., Arabagi V., Sitti M.: 'Free flight simulations and pitch and roll control experiments of a sub-gram flapping-flight micro aerial vehicle'. IEEE Int. Conf. on Robotics and Automation (ICRA), Shanghai, People's Republic of China, May 2011, pp. 1–7
[10] Wood R.J., Avadhanula S., Sahai R., *ET AL.*: 'Microrobot design using fiber reinforced composites', *J. Mech. Des.*, 2008, **130**, (5), p. 052304
[11] Ellington C.P.: 'The aerodynamics of hovering insect flight. II. Morphological parameters', *Philos. Trans. R. Soc. B*, 1984, **305**, (1122), pp. 17–40
[12] Wood R.J., Cho K.J., Hoffman K.: 'A novel multi-axis force sensor for microrobotics applications', *Smart Mater. Struct.*, 2009, **18**, (12), p. 125002
[13] Finio B.M., Wood R.J.: 'Optimal energy density piezoelectric twisting actuators'. IEEE Int. Conf. on Intelligent Robots and Systems (IROS), San Francisco, CA, USA, September 2011, pp. 384–389
[14] Finio B.M., Galloway K.C., Wood R.J.: 'An ultra-high precision, high bandwidth torque sensor for microrobotics applications'. IEEE Int. Conf. on Intelligent Robots and Systems (IROS), San Francisco, CA, USA, September 2011, pp. 31–38
[15] Oppenheimer M.W., Doman D.B., Sigthorsson D.O.: 'Dynamics and control of a biomimetic vehicle using biased wingbeat forcing functions', *J. Guid. Control Dyn.*, 2011, **34**, (1), pp. 204–217